Spin eigenmodes of magnetic skyrmions and the problem of the effective skyrmion mass

Volodymyr P. Kravchuk,[1,2,*] Denis D. Sheka,[3,†] Ulrich K. Rößler,[2,‡] Jeroen van den Brink,[2,4,§] and Yuri Gaididei[1,‖]

[1]*Bogolyubov Institute for Theoretical Physics, National Academy of Sciences of Ukraine, 03680 Kyiv, Ukraine*

[2]*Leibniz-Institut für Festkörper- und Werkstoffforschung, IFW Dresden, 01171 Dresden, Germany*

[3]*Department of Mathematics and Theoretical Radio Physics, Faculty of Radio Physics, Electronics and Computer Systems, Taras Shevchenko National University of Kyiv, 01601 Kyiv, Ukraine*

[4]*Institute for Theoretical Physics, TU Dresden, 01069 Dresden, Germany*

(Received 29 November 2017; published 7 February 2018)

The properties of magnon modes localized on a ferromagnetic skyrmion are studied. Mode eigenfrequencies display three types of asymptotic behavior for large skyrmion radius R_s, namely, $\omega_0 \propto R_s^{-2}$ for the breathing mode and $\omega_{-|\mu|} \propto R_s^{-1}$ and $\omega_{|\mu|} \propto R_s^{-3}$ for modes with negative and positive azimuthal quantum numbers, respectively. A number of properties of the magnon eigenfunctions are determined. This enables us to demonstrate that the skyrmion dynamics for a traveling-wave ansatz obeys the massless Thiele equation.

DOI: 10.1103/PhysRevB.97.064403

I. INTRODUCTION

Chiral magnetic skyrmions [1–9] are particlelike topological solitons with an integer topological charge (skyrmion number). In contrast to a magnetic vortex [10–12], which has half-integer topological charge, the skyrmion is a truly localized excitation. As a consequence, the dynamics of the skyrmion is insensitive to the size and shape of a sufficiently large sample, and remote skyrmions do not interact with each other, apart from weak stray field effects. This is in strong contrast to magnetic vortices. The possibility to manipulate skyrmions as "individual particles" together with the topological stability of these "particles" has prompted a large number of studies in recent years, where skyrmions are considered key elements for nonvolatile memory and logic devices [3,13–17]. This perspective has instigated a new area of spintronics: skyrmionics [16].

On the other hand, magnon spintronics [18] is another recently emerging area of spintronics which is intensively developing in parallel to skyrmionics. Magnon transistors [19] and a number of wave-based logic devices [18,20] are proposed as key elements for wave-based computing [18]. In this regard, the combination of these two trends, skyrmion-based nonvolatile memory and magnon-based logic devices, could significantly advance the development of magnetic computer elements as an alternative to charge-based semiconductor technology. However, the concept of a spin-wave- and skyrmion-based spintronics requires a deep understanding of the skyrmion magnon modes.

The spectrum of linear excitations of any system reflects its fundamental properties; for example, the spectrum describes conditions for instabilities and allows us to analyze their types. Knowledge of spectral properties also opens great opportunities for resonance experiments [21–23]. The presence of skyrmion resonances can be considered proof of the presence of skyrmions in a system if one knows the distinctive features of its excitation spectrum, and values of the eigenfrequencies can be used for the determination of materials parameters.

Due to the fundamental interest and importance for applications many studies of magnon spectra of skyrmions were recently carried out [24–33]. However, most of these studies are numerical, and the existing theories are far from complete. Some important questions are still unclear, e.g., the presence of the high-frequency gyrotropic mode, which is a counterpart of the translational zero mode. It has the same azimuthal symmetry but nonzero eigenfrequency. In some models this mode is responsible for the formal appearance of the mass of the topological soliton [11,29,30,34–41] (see discussion in Sec. V). In most of the mentioned studies this mode was not found [24–27]. On the other hand, it was found for some cases of large-radius skyrmions [29–31].

In this paper we present a detailed study and classification of the skyrmion magnon spectrum. This paper is organized as follows. Section II explains our model and introduces a system of dimensional units (see Table I). In Sec. III we consider the simplest case of the radially symmetrical magnon mode, the so-called breathing mode. A general study of the magnon spectrum is presented in Sec. IV. Here, we obtain the asymptotic behavior of the eigenfrequencies of all localized modes. Additionally, we describe various properties of the mode eigenfunctions, e.g., the orthogonality condition. These properties are employed in Sec. V, where the skyrmion dynamics within the traveling-wave model is described by the approach of collective variables. Here, we demonstrate the skyrmion dynamics obeys the *massless* Thiele equation.

II. MODEL AND STATIC EQUILIBRIUM SOLUTIONS

Here, we consider the case of a chiral skyrmion, which is stabilized in a ferromagnetic film with a perpendicular easy anisotropy axis and in the absence of external magnetic fields.

*Corresponding author: vkravchuk@bitp.kiev.ua
†sheka@knu.ua
‡u.roessler@ifw-dresden.de
§j.van.den.brink@ifw-dresden.de
‖ybg@bitp.kiev.ua

 ©2018 American Physical Society

TABLE I. Units of physical quantities used in this paper. Values are calculated for the following material parameters: $A = 1.6\times10^{-11}$ J/m, $M_s = 1.1\times10^{6}$ A/m, and $K = K_0 - \frac{\mu_0}{2}M_s^2 = 5.1\times10^{5}$ J/m^3, with $K_0 = 1.27\times10^{6}$ J/m^3 being the intrinsic magnetocrystalline anisotropy.

Quantity	Unit of measurement	Value for Pt/Co/AlO$_x$ layer structure [42]
Length	$\ell = \sqrt{A/K}$	5.6 nm
Time	$\Omega_0^{-1} = \left(\frac{2K\gamma}{M_s}\right)^{-1}$	6.12 ps ($\Omega_0 = 26$ GHz)
Energy	$E_{\mathrm{BP}} = 8\pi AL$	4×10^{-19} J (for $L = 1$ nm)
Mass	$\mathcal{M}^{\star} = L\frac{M_s^2}{K\gamma^2}$	7.6×10^{-26} kg (for $L = 1$ nm)
DMI strength	$\sigma = \sqrt{AK}$	2.9 mJ/m^2

The advantage of the field-free case is that the skyrmion can have an arbitrarily large radius. The problem of the magnon spectrum has still not been studied systematically for this case.

In our model we take into account three contributions to the total energy of the ferromagnetic film,

$$E = L\int\left[A\mathscr{E}_{\mathrm{ex}} + K\left(1-m_z^2\right) + D\mathscr{E}_{\mathrm{D}}\right]dS, \tag{1}$$

where the integration is performed over the film area and L is the film thickness, which is assumed to be small enough to ensure uniformity of the magnetization in the perpendicular direction. The first term of the integrand is the exchange energy density with $\mathscr{E}_{\mathrm{ex}} = \sum_{i=x,y,z}(\partial_i \boldsymbol{m})^2$, and A is the exchange constant. Here, $\boldsymbol{m} = \boldsymbol{M}/M_s$ is the unit magnetization vector, with M_s being the saturation magnetization. The second term is the perpendicular easy-axis anisotropy with $K > 0$, and $m_z = \boldsymbol{m}\cdot\hat{\boldsymbol{z}}$ is the magnetization component normal to the surface. Here, we assume that the introduced uniaxial anisotropy incorporates an effective easy-plane contribution, which derives from magnetostatics. This assumption is valid for the case of ultrathin films [43,44]. The last term represents the Dzyaloshinskii-Moriya interaction (DMI), with $\mathscr{E}_{\mathrm{D}} = m_z\nabla\cdot\boldsymbol{m} - \boldsymbol{m}\cdot\nabla m_z$. This inhomogeneous DMI is associated with the $C_{\infty v}$ symmetry of (idealized) ultrathin films [6,8,45,46] or bilayers [47], stems from the relativistic spin-orbit coupling [48,49], and selects a fixed sense of rotation for any twisted noncollinear magnetization configuration.

In the following we introduce a system of dimensionless units, explained in the Table I. The proposed units have the following physical meaning: the magnetic length ℓ is the typical width of a domain wall in the given system with vanishing DMI, σ is the energy per unit area of such a domain wall, E_{BP} is the energy of the Belavin-Polyakov soliton [50], which coincides with the energy of a skyrmion with an infinitesimally small radius, and Ω_0 is the frequency of the uniform ferromagnetic resonance, where $\gamma = g\mu_{\mathrm{B}}/\hbar$ is the gyromagnetic ratio, with g being the Landé g factor, μ_{B} being the Bohr magneton, and $\hbar$ being Planck's constant.

The constraint $|\boldsymbol{m}| = 1$ is encoded using the spherical angular parametrization $\boldsymbol{m} = \sin\theta\cos\phi\hat{\boldsymbol{x}} + \sin\theta\sin\phi\hat{\boldsymbol{y}} + \cos\theta\hat{\boldsymbol{z}}$. Magnetization dynamics is described by the Landau-Lifshitz equations

$$\sin\theta\dot{\phi} = 4\pi\frac{\delta\mathcal{E}}{\delta\theta}, \quad \sin\theta\dot{\theta} = -4\pi\frac{\delta\mathcal{E}}{\delta\phi}, \tag{2}$$

where the dot denotes the derivative with respect to the dimensionless time $\tau = t\Omega_0$ and $\mathcal{E} = E/E_{\mathrm{BP}}$ is the dimensionless energy. Here and below, all distances are measured in units of ℓ, in accordance with Table I.

For the proposed system of units the dimensionless DMI constant $d = D/\sigma$ is the only parameter which controls the system. The described model is characterized by the critical value of the DMI constant $d_0 = 4/\pi$, which separates two ground states, namely, the uniform state $\boldsymbol{m} = \pm\hat{\boldsymbol{z}}$ for the case $|d| < d_0$ and the periodic helical state for $|d| > d_0$ [5,7,42,49,51,52]. For the case $0 < |d| < d_0$ Eqs. (2) have a stationary skyrmion solution $\theta = \Theta(\rho)$ and $\phi = \Phi(\chi)$, where $\Phi = \chi + \Psi_0$ and $\{\rho,\chi\}$ are polar coordinates. This is an excitation of the uniform ground state. The skyrmion profile is determined by [5–7,42,52]

$$\nabla_\rho^2\Theta - \sin\Theta\cos\Theta\left(1+\frac{1}{\rho^2}\right) + \frac{|d|}{\rho}\sin^2\Theta = 0, \tag{3a}$$

$$\Theta(0) = \pi, \quad \Theta(\infty) = 0, \tag{3b}$$

where $\nabla_\rho^2 f = \rho^{-1}\partial_\rho(\rho\,\partial_\rho f)$ is the radial part of the Laplace operator. For the case of boundary conditions (3b) $\Psi_0 = 0$ if $d > 0$, and $\Psi_0 = \pi$ if $d < 0$. In other words, the considered type of DMI stabilizes a so-called Néel (hedgehog) skyrmion. The case of alternative boundary conditions $\Theta(0) = 0$ and $\Theta(\infty) = \pi$ is not considered here because it does not result in fundamentally new properties of the magnon spectra compared to (3b).

III. LARGE-RADIUS SKYRMION AND RADIALLY SYMMETRICAL MODE

The skyrmion profile is a localized function [5,7,42,52], which enables one to introduce the skyrmion radius R_s as a solution of the equation $\cos\Theta(R_s) = 0$. The skyrmion radius R_s strongly depends on the DMI constant [7,42]: $R_s \to 0$ when $d \to 0$ (skyrmion collapse), while $R_s \to \infty$ when $d \to \pm d_0$ [see Fig. 1(a)]. For a skyrmion with a large radius $R_s \gg 1$ one can easily estimate the asymptotic behavior of R_s. In this case the skyrmion profile is well described by the circular domain wall ansatz

$$\cos\theta = \tanh\frac{\rho - R_s}{\Delta}, \quad \phi = \chi + \Psi\,. \tag{4}$$

Here, the skyrmion radius R_s, phase Ψ, and width Δ are treated as collective variables. This is in contrast to some

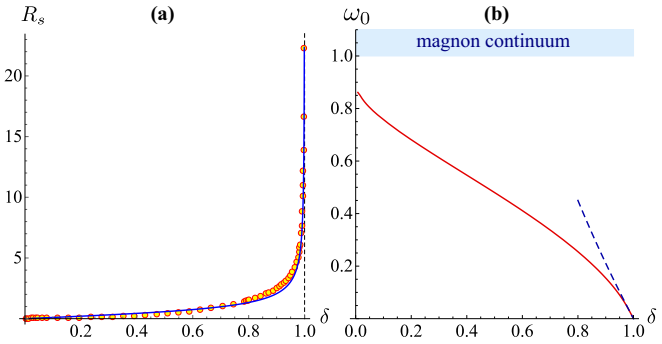

FIG. 1. (a) Skyrmion radius as a function of the normalized DMI constant. The line shows the approximation (6), while dots correspond to the exact numerical solutions of the differential problem (3). (b) Breathing-mode eigenfrequency (solid line) and asymptotics (9) (dashed line) for the case of a large skyrmion radius ($\delta \lessapprox 1$).

previous papers [29,38,42], where the model (4) was used for constant Δ. The normalized energy of the skyrmion as described by the model (4) reads

$$\mathcal{E} \approx \frac{1}{2}\left(\underbrace{\frac{R_s}{\Delta} + \frac{\Delta}{R_s}}_{\text{exchange}} \underbrace{- 2\delta R_s \cos\Psi}_{\text{DMI}} + \underbrace{\Delta R_s}_{\text{anisotr.}} \right), \tag{5}$$

where $\delta = d/d_0$ is the normalized DMI constant. A minimum of the energy (5) is reached for the following equilibrium values of the collective variables: $\Delta_0 = |\delta|$ and $\Psi_0 = 0$ ($\Psi_0 = \pi$) when $\delta > 0$ ($\delta < 0$). And the skyrmion radius reads

$$R_s \approx |\delta|/\sqrt{1-\delta^2}. \tag{6}$$

In the limit $\delta \to 1$ the estimate (6) transforms into the previously proposed behavior [42], $R_s \approx 1/\sqrt{2(1-\delta)}$, which was obtained for constant width, $\Delta = 1$. The approximate radius agrees well with the exact values of R_s for the whole range of the DMI constant, not only for the case $R_s \gg 1$ [see Fig. 1(a)].

Let us now consider excitation of the radially symmetrical mode. This can be easily done by considering the time-dependent dynamics of the collective variables $R_s(t)$ and $\Psi(t)$ in the vicinity of their equilibrium values. To this end we treat the equations of motion (2) as extrema of the action functional $S = \int \mathcal{L} d\tau$ with the Lagrange function

$$\mathcal{L} = \frac{1}{4\pi}\int (1-\cos\theta)\,\dot{\phi}\, d\mathcal{S} - \mathcal{E}. \tag{7}$$

Ansatz (4) represents a circularly closed domain wall. It is well known [53–57] that dynamics of the width Δ of the one-dimensional domain wall has an essentially different time scale compared to the time scale of the domain wall position R_s and phase Ψ. Namely, Δ quickly relaxes towards its equilibrium value determined by the much slower variables R_s and Ψ. Therefore, the assumption that Δ is a "slave" variable works very well in most cases. Here, we assume that the same is true for the circularly closed domain wall if $R_s \gg 1$. In this case the substitution of ansatz (4) into (7) results in the following effective Lagrange function:

$$\mathcal{L}^{\text{eff}} = \dot{\Psi}\, R_s^2 - \mathcal{E}^{\text{eff}},$$
$$\mathcal{E}^{\text{eff}} = R_s\left(\frac{1}{|\delta|} - 2\delta\cos\Psi + |\delta|\right) + \frac{|\delta|}{R_s}. \tag{8}$$

As follows from (8), the skyrmion area is the canonically conjugated momentum for the skyrmion phase. The effective Lagrange function (8) generates a set of two equations of motion for Ψ and R_s, which have static equilibrium solutions (6) and Ψ_0 as determined above. The corresponding linear dynamics in the vicinity of the equilibrium state is characterized by the eigenfrequency

$$\omega_0 = \frac{1-\delta^2}{|\delta|} = \frac{1}{R_s\sqrt{1+R_s^2}} \approx \frac{1}{R_s^2}. \tag{9}$$

The corresponding asymptotics is shown in Figs. 1(b) and 2(b).

IV. GENERAL DESCRIPTION OF THE MAGNON SPECTRA

The dispersion relation of linear excitations (magnons) of the uniform ground state is not influenced by the DMI and coincides with the common dispersion for the easy-axis magnets $\omega = 1 + q^2$, with $q = k\ell$ being the dimensionless wave number. Thus, one has a continuum spectrum with $\omega \geqslant 1$ for frequencies above the anisotropy-induced gap. In the following we are interested in magnons over the equilibrium skyrmion state. For this purpose we introduce small excitations of the stationary solution: $\theta = \Theta + \vartheta$, $\phi = \Phi + \varphi/\sin\Theta$. Equations (2) linearized with respect to the excitations result in

$$\dot{\varphi} = -\nabla^2\vartheta + U_1\vartheta + W\partial_\chi\varphi, \tag{10a}$$
$$-\dot{\vartheta} = -\nabla^2\varphi + U_2\varphi - W\partial_\chi\vartheta. \tag{10b}$$

Here, the Laplace operator has the form $\nabla^2 = \nabla_\rho^2 + \rho^{-2}\partial_{\chi\chi}^2$, and the "potentials" are as follows:

$$U_1 = \cos 2\Theta\left(1+\frac{1}{\rho^2}\right) - \frac{|d|}{\rho}\sin 2\Theta,$$
$$U_2 = \cos^2\Theta\left(1+\frac{1}{\rho^2}\right) - \Theta'^2 - |d|\left(\Theta' + \frac{\sin\Theta\cos\Theta}{\rho}\right),$$
$$W = \frac{2}{\rho^2}\cos\Theta - \frac{|d|}{\rho}\sin\Theta. \tag{10c}$$

Here, a prime denotes the derivative with respect to ρ. Equations (10) have the solution $\vartheta(\rho,\chi,\tau) = f(\rho)\cos(\omega\tau + \mu\chi + \eta)$, $\varphi(\rho,\chi,\tau) = g(\rho)\sin(\omega\tau + \mu\chi + \eta)$, where the azimuthal wave number $\mu \in \mathbb{Z}$ determines the node number ($2|\mu|$) when moving around the skyrmion center in the azimuthal direction and η is an arbitrary phase. The eigenfrequencies ω and the corresponding eigenfunctions f, g are determined by the following eigenvalue problem (EVP):

$$H\boldsymbol{\psi} = \omega\sigma_x\boldsymbol{\psi} \tag{11a}$$

for a Hermitian operator

$$H = \begin{pmatrix} -\nabla_\rho^2 + \frac{\mu^2}{\rho^2} + U_1 & \mu W \\ \mu W & -\nabla_\rho^2 + \frac{\mu^2}{\rho^2} + U_2 \end{pmatrix}. \tag{11b}$$

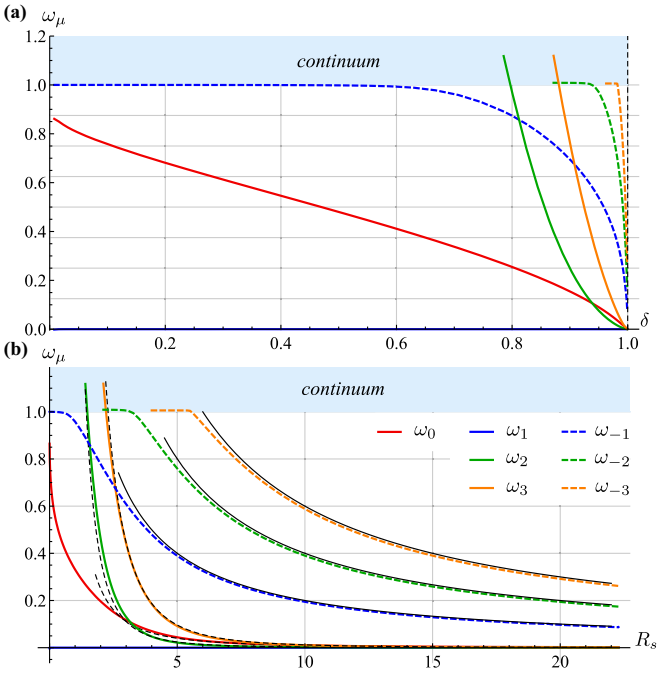

FIG. 2. The eigenfrequencies ω_μ of localized modes as functions of (a) the normalized DMI constant $\delta = d/d_0$ and (b) skyrmion radius are obtained from numerical solution of the EVP (11). Thin lines are the asymptotes (13) for the case $R_s \gg 1$. Modes with $|\mu| > 3$ are not shown. Frequency ω_1 belongs to the zero translational mode, while ω_{-1} corresponds to the high-frequency gyrotropic mode.

Here, $\boldsymbol{\psi} = (f,g)^{\mathrm{T}}$, and σ_x is the first Pauli matrix. The formulated EVP (11) structurally coincides with the corresponding EVP previously formulated for the case of magnons over precessional solitons in easy-axis magnets [38–40], magnetic vortices in easy-plane magnets [37,58], and magnetic skyrmions [24–27]. Note that there is an alternative formulation of (10) in the form of the generalized Schrödinger equation [39,58] (see Appendix B for details).

The EVP (11) is analyzed both analytically and numerically (for details see Appendix A). Equations (11) are invariant with respect to the simultaneous change of sign of three quantities: $\omega \to -\omega$, $\mu \to -\mu$, and $f \to -f$ (or $g \to -g$). This invariance results in a symmetry of the spectrum, which simplifies classification of the modes: one can fix either the sign of μ considering both signs of ω or the sign of ω considering both signs of μ. Following the previous studies [24,37–39,58], we choose the latter classification and consider non-negative frequencies $\omega \geqslant 0$.

A number of localized modes are found below the edge of the continuum spectrum. Frequencies of the localized modes strongly depend on the DMI constant [see Fig. 2(a)]; alternatively, we demonstrate the dependence on the skyrmion radius [Fig. 2(b)], which can be useful for applications. For any value of the skyrmion radius (DMI constant) there are at least three localized modes: the radially symmetrical (breathing) mode $|\mu = 0\rangle$ and two modes $|\pm 1\rangle$ which are called gyrotropic [41]. Due to the translational invariance one of the gyrotropic modes has zero eigenfrequency $\omega_1 = 0$ (in our case this is the mode $|+1\rangle$). This mode is called translational; it has the following eigenfunctions [59]: $f_1 = -\Theta'$ and $g_1 = \sin\Theta/\rho$ (see Fig. 3). Although the other gyrotropic mode $|-1\rangle$ has the same azimuthal symmetry as the translational one, its eigenfunctions f_{-1} and g_{-1} are completely different (see Fig. 3). For a small-radius skyrmion the eigenfrequency ω_{-1} of the mode $|-1\rangle$ practically coincides with the edge of the continuum, while for large skyrmions it is inversely proportional to the skyrmion radius [see Fig. 2(b)]. It is natural to call the mode $|-1\rangle$ the high-frequency gyrotropic mode.

With the skyrmion radius increasing, the localized modes with higher azimuthal numbers $|\mu| \geqslant 2$ appear in the gap. However, it is important to note that for a given μ there is no more than one localized mode. Some examples of eigenfunctions of other localized modes are shown in Fig. 3. Far from the skyrmion the functions f_μ and g_μ have the same asymptotic behavior because $U_1 \to U_2$ when $\rho \to \infty$. Note also that the localization area of the eigenfunctions increases when the corresponding eigenfrequency reaches the bottom of the continuum.

The eigenfunctions f_μ and g_μ have several properties, which are important for further analysis. Here, we present the orthogonality condition

$$\int_0^\infty \rho[f_\mu g_{-\mu} - f_{-\mu} g_\mu]d\rho = 0, \tag{12}$$

which follows from (A3) when the symmetry between branches μ and $-\mu$ is taken into account (for details see Appendix A). The analogous orthogonality condition was previously obtained for magnons over precessional solitons [40]. Other properties are listed in (A5), (A6), (A8), and (A11).

The properties of the eigenfunctions enable us to find the eigenfrequency asymptotics for the case of a large-radius

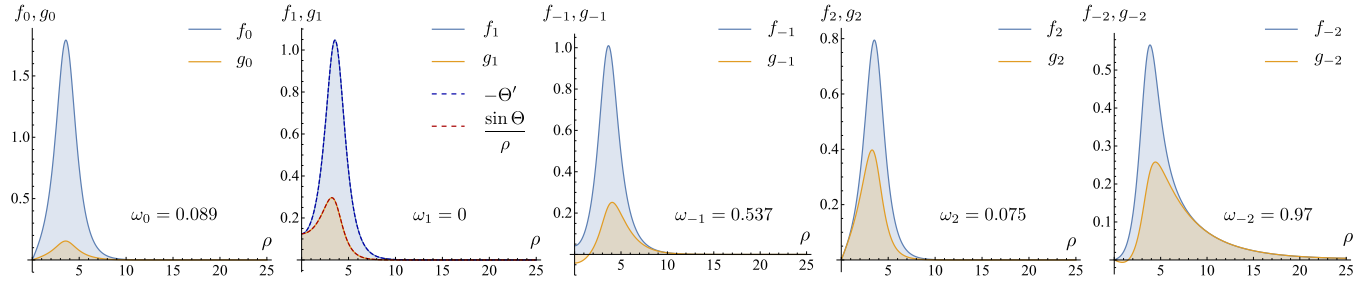

FIG. 3. Eigenfunctions and eigenfrequencies obtained from the numerical solution of (11) for the case $\delta = 0.95$ ($R_s = 3.51$) and free boundary conditions. The eigenfunctions are normalized by the rule $\alpha_\mu = 2$.

skyrmion with $R_s \gg 1$:

$$\omega_0 \approx \frac{1}{R_s^2}, \quad \omega_\mu \approx \begin{cases} 2|\mu|/R_s, & \mu < 0, \\ c_\mu/R_s^3, & \mu > 0, \end{cases} \tag{13}$$

where c_μ is a constant (for details see Appendix A). Comparison with the numerical solution justifies the assumption that $c_\mu = \mu(\mu^2-1)/2$. The asymptotics (13) are shown in Fig. 2 by thin lines.

For the case $|\delta| \to 1$ (or, equivalently, $R_s \to \infty$) the number of local modes grows infinitely. In the critical point $|\delta| = 1$ all the modes become unstable (the frequencies of these modes vanish). The skyrmion instabilities at point $|\delta| = 1$ for zero field were predicted earlier for the particular cases $\mu = 0$ (radial instability) [60] and $|\mu| = 2$ (elliptical instability) [61].

V. EFFECTIVE SKYRMION MASS IN THE APPROACH OF COLLECTIVE VARIABLES

Since the skyrmion is an exponentially localized excitation, there is a notion that its dynamics can be approximated by the dynamics of a point particle with coordinates $\mathcal{R} = \{\mathcal{X},\mathcal{Y}\}$, which are called collective coordinates. However, the definition of the skyrmion center $\mathcal{R}$ is not unique. The essential dependence of the collective coordinate dynamics on the definition of $\mathcal{R}$ was already indicated in Ref. [40] for the example of the precessional solitons. A recent analysis of numerically simulated skyrmion motion shows [52] that the different definitions result in essentially different types of trajectories $\mathcal{R}(\tau)$. In order to describe more complicated trajectories the internal degrees of freedom of the skyrmion must be taken into consideration [29], which results in the appearance of an effective-mass term in the equations of motion for the collective coordinates [29,41]. The aim of this section is to utilize the properties of the magnon eigenfunctions in order to (i) determine a physically sound definition of the skyrmion center and (ii) clarify the appearance of the effective-mass term.

Collective-variable approaches [62] are widely used to analyze the dynamics of solitonlike excitations in magnetic media [11,57,63–65]. They are based on the assumption that the time dependence of the continuum magnetization vector field $\boldsymbol{m}$ can be reduced to the time dependence of a discrete set of collective variables $\boldsymbol{\xi} = \{\xi_1,\xi_2,\dots\}$, i.e., $\boldsymbol{m}(\boldsymbol{r},\tau) = \boldsymbol{m}(\boldsymbol{r},\boldsymbol{\xi}(\tau))$. This enables one to proceed from the coupled partial differential equations (2) to a set of the ordinary differential equations

$$\sum_j G_{\xi_i\xi_j}\dot{\xi}_j = \frac{\partial \mathcal{E}}{\partial \xi_i},$$
$$G_{\xi_i\xi_j} = \frac{1}{4\pi}\int \sin\theta\left(\frac{\partial\theta}{\partial\xi_i}\frac{\partial\phi}{\partial\xi_j} - \frac{\partial\theta}{\partial\xi_j}\frac{\partial\phi}{\partial\xi_i}\right)d\mathcal{S}, \tag{14}$$

where $d\mathcal{S} = dS/\ell^2$ is a dimensionless area element. See also the tutorial papers [11,53].

A case where the only variables are collective coordinates describing the placement of a soliton ($\boldsymbol{\xi} = \mathcal{R}$) is called the traveling-wave model $\boldsymbol{m}(\boldsymbol{r},\tau) = \boldsymbol{m}_0(\boldsymbol{r} - \mathcal{R}(\tau))$, where $\boldsymbol{m}_0$ is a stationary solution. Let us consider a more general ansatz:

$$\theta^{\rm an}(\rho,\chi,\tau) = \Theta(\rho) + \sum_{\mu=-\infty}^{\infty} f_\mu(\rho)[\mathcal{A}_\mu(\tau)\cos\mu\chi + \mathcal{B}_\mu(\tau)\sin\mu\chi],$$
$$\phi^{\rm an}(\rho,\chi,\tau) = \chi + \Psi_0 + \frac{1}{\sin\Theta(\rho)} \times \sum_{\mu=-\infty}^{\infty} g_\mu(\rho)[\mathcal{A}_\mu(\tau)\sin\mu\chi - \mathcal{B}_\mu(\tau)\cos\mu\chi], \tag{15}$$

which corresponds to (A4) but where only localized modes are taken into account. Here, $\Theta(\rho)$ determines the static skyrmion profile. The time-dependent collective variables $\mathcal{A}_\mu$, $\mathcal{B}_\mu$ play the role of the amplitudes of the magnon modes. Thus, in our case $\boldsymbol{\xi} = \{\mathcal{A}_k,\mathcal{B}_k\}$, with $k \in \mathbb{Z}$.

First of all, it is important to note that the ansatz (15) includes the infinitesimal skyrmion displacements in the spirit of the traveling-wave model. Indeed, the expansion of expressions

$$\theta = \Theta(\sqrt{(x-\mathcal{X})^2 + (y-\mathcal{Y})^2}),$$
$$\phi = \arctan\frac{y-\mathcal{Y}}{x-\mathcal{X}} + \Psi_0 \tag{16}$$

in $\mathcal{X},\mathcal{Y}$ up to the linear terms and comparison with (15) result in

$$\mathcal{X} = \mathcal{A}_1, \quad \mathcal{Y} = \mathcal{B}_1 \tag{17}$$

if the form of the eigenfunctions $f_1 = -\Theta'(\rho)$ and $g_1 = \sin\Theta(\rho)/\rho$ is taken into account.

The second important observation is that the collective coordinates, which correspond to the traveling-wave model, coincide with the first moment (center of mass) of the topological density:

$$\mathcal{R} = \frac{1}{4\pi\mathcal{Q}}\int \boldsymbol{r}\,\mathcal{J}\,d\mathcal{S}, \tag{18}$$

where $\mathcal{J} = -\boldsymbol{m}\cdot[\partial_x\boldsymbol{m}\times\partial_y\boldsymbol{m}]$ is the topological charge density and $\mathcal{Q} = (4\pi)^{-1}\int\mathcal{J}\,d\mathcal{S}$ is the total topological charge of the skyrmion [66]. Expression (18) directly follows from (15) and (17) if the orthogonality property (12) of the eigenfunctions is considered. The definition of the skyrmion center in the form of (18) was used in a number of papers [12,52,67–70].

Let us obtain the collective-variable equations (14) in the approximation that is linear with respect to ξ_i and $\dot{\xi}_i$. For this purpose we substitute the ansatz (15) into (14) and perform the integration using the orthogonality property (12) of the eigenfunctions. Finally, we obtain the following components of the gyrotensor:

$$G_{\mathcal{A}_\mu\mathcal{A}_{\mu'}} = G_{\mathcal{B}_\mu\mathcal{B}_{\mu'}} = 0, \quad G_{\mathcal{A}_\mu\mathcal{B}_{\mu'}} = -\frac{\alpha_\mu}{2}\delta_{\mu,\mu'}, \tag{19}$$

where $\alpha_\mu = \int_0^\infty \rho f_\mu g_\mu d\rho$. Note that $\alpha_1 = 2\mathcal{Q}$. The effective energy corresponding to the model (15) has the form (up to the second-order terms in $\mathcal{A}_\mu$ and $\mathcal{B}_\mu$)

$$\mathcal{E} = \frac{1}{8}\sum_\mu \varepsilon_\mu\left(\mathcal{A}_\mu^2 + \mathcal{B}_\mu^2\right) + \mathcal{E}_0. \tag{20}$$

Here, $\varepsilon_\mu = \varepsilon_\mu^f + \varepsilon_\mu^g$ [see (A7)], and $\mathcal{E}_0$ is a contribution to the energy which is independent of the collective variables. Expression (20) is a result of the straightforward integration of the energy (1) using the property (A8).

Substituting (19) and (20) into (14), one obtains the set of equations for collective coordinates:

$$\begin{aligned} \xi_i = \mathcal{A}_1: &\quad \dot{\mathcal{B}}_1 = 0, \\ \xi_i = \mathcal{B}_1: &\quad \dot{\mathcal{A}}_1 = 0, \\ \xi_i = \mathcal{A}_{\mu\neq 1}: &\quad \dot{\mathcal{B}}_\mu = -\omega_\mu \mathcal{A}_\mu, \\ \xi_i = \mathcal{B}_{\mu\neq 1}: &\quad \dot{\mathcal{A}}_\mu = \omega_\mu \mathcal{B}_\mu, \end{aligned} \tag{21}$$

where the properties (A5) and (A11) were utilized. Following the terminology of Ref. [30], one can conclude from (21) that the mode $|1\rangle$ is a *special zero normal mode*, which, in contrast to *inertial zero normal mode* [30], does not lead to mass generation. Introducing now a driving potential $\mathcal{E} \to \mathcal{E} + \mathcal{U}(\mathcal{X},\mathcal{Y})$, which is assumed to be small enough not to change the eigenfunctions significantly, and taking into account (17), one obtains from (14) the well-known Thiele equation for a massless particle [11,57,63]:

$$[\boldsymbol{e}_z \times \dot{\boldsymbol{\mathcal{R}}}] - \partial_{\boldsymbol{\mathcal{R}}} \mathcal{U} = 0. \tag{22}$$

Earlier it was shown [71] that in the absence of external driving the translational mode of the magnetic vortex in an easy-plane ferromagnet does not exist. In other words, the zero translational mode is not inertial [30] for this case. The same results are valid for the case of magnetic skyrmion in a ferromagnetic film with the perpendicularly oriented easy axis when the analysis proposed in Ref. [71] is applied. Thus, the inertial mass term is not expected in equations for collective coordinates for the case of a ferromagnetic vortex or for the ferromagnetic skyrmion. This is in contrast to the cases of antiferromagnets [72] and weak ferromagnets [73], where the mass term appears in a natural way since the second-order time derivative is initially present in the equation of motion written in terms of the Néel order parameter [74–77]. However, the inertial mass term is often used in collective-coordinate equations for ferromagnetic vortices [11,34–37], precessional solitons [38–40,78], and skyrmions [9,29,41]. In part, this ambiguity originates from alternative methods of definitions of the soliton center. A frequently used method is based on the first moment of the perpendicular magnetization component [29,30,41,52]

$$\mathbf{R} \equiv (\mathrm{X},\mathrm{Y}) = \frac{\int \boldsymbol{r}(1-m_z)d\mathcal{S}}{\int (1-m_z)d\mathcal{S}}. \tag{23}$$

Thus, $\mathbf{R}$ signifies the "center of mass" of the m_z distribution. Using (15), one obtains (in a linear approximation in amplitudes $\mathcal{A}_i$, $\mathcal{B}_i$)

$$X = c_1\mathcal{A}_1 + c_{-1}\mathcal{A}_{-1}, \quad Y = c_1\mathcal{B}_1 - c_{-1}\mathcal{B}_{-1}, \tag{24}$$

where $c_i = \frac{1}{2}\int_0^\infty \rho^3 g_1(\rho) f_i(\rho) d\rho / \int_0^\infty \rho[1-\cos\Theta(\rho)]d\rho$. In this way a formal coupling between modes $|1\rangle$ and $|-1\rangle$ is introduced into the system, and as a result, an effective-mass term appears [29,30]. Indeed, excluding amplitudes $\mathcal{A}_{-1}$ and $\mathcal{B}_{-1}$ from Eqs. (14) and (24), one obtains a set of second-order ordinary differential equations for X and Y. For the case of a radially symmetrical potential $\mathcal{U} = \omega_{\mathrm{G}}\mathcal{R}^2/2$ they can be written in the vector form

$$\mathcal{M}\ddot{\mathbf{R}} - [\boldsymbol{e}_z \times \dot{\mathbf{R}}] + k\mathbf{R} = 0, \tag{25}$$

where $\mathcal{M} = 1/(\omega_{-1} - \omega_{\mathrm{G}})$ and $k = \omega_{-1}\omega_{\mathrm{G}}/(\omega_{-1} - \omega_{\mathrm{G}})$. However, it should be emphasized that treatment of the position vector $\mathbf{R} \neq \mathcal{R}$ as a skyrmion collective coordinate is not physically sound because $\mathbf{R}$ does not describe the skyrmion displacement in the sense of the traveling-wave model.

Note that here we take into account only the localized modes. Recently, it was predicted that a skyrmion driven by the spin Hall torque could display an inertial behavior due to the delocalized modes of the continuum [79]. Also in quantum systems, a ferromagnetic skyrmion can behave as a massive particle in the presence of defects or a potential trap [80].

VI. CONCLUSIONS

The main results of this paper are as follows: (i) We obtained the asymptotic behavior of localized magnon modes over the chiral skyrmion [see (13)]. (ii) The high-frequency gyrotropic mode is always present in the spectrum; however, its frequency practically coincides with the edge of the magnon continuum, except in the vicinity of the critical point $|d| = 4/\pi$. (iii) Using the orthogonality relation (12) for the magnon eigenfunctions, we showed that the collective skyrmion coordinates, which describe its motion in terms of a traveling-wave model, coincide with the first moment of the topological charge distribution. (iv) In terms of these collective coordinates the skyrmion dynamics is massless.

ACKNOWLEDGMENTS

V.P.K. and D.D.S. acknowledge the Alexander von Humboldt Foundation for the support. This work has been supported by the Deutsche Forschungsgemeinschaft via SFB 1143.

APPENDIX A: PROPERTIES OF THE MAGNON SPECTRUM

For each given value of μ the EVP (11) generates a "ν spectrum," which is described by the eigenfunctions $f_{\mu,\nu}$ and $g_{\mu,\nu}$ with the corresponding eigenfrequencies $\omega_{\mu,\nu}$. They are determined by the EVP

$$\mathcal{H}_\mu \boldsymbol{\psi}_\mu = \omega_\mu \boldsymbol{\psi}_\mu, \tag{A1}$$

where $\boldsymbol{\psi}_\mu = (f_\mu, g_\mu)^{\mathrm{T}}$ and $\mathcal{H}_\mu = \sigma_x H$ [see (11b)]. Operator $\mathcal{H}_\mu$ is Hermitian in the Hilbert space $\mathbb{H}^\mu$ with the scalar product

$$\langle \boldsymbol{\psi}_{\mu,\nu} | \boldsymbol{\psi}_{\mu,\nu'} \rangle \equiv \int_0^\infty \rho\, \boldsymbol{\psi}_{\mu,\nu}^{\mathrm{T}} \sigma_x \boldsymbol{\psi}_{\mu,\nu'}\, d\rho. \tag{A2}$$

This results in real-valued eigenfrequencies $\omega_{\mu,\nu}$, and (A2) enables us to formulate the orthogonality condition (for the given μ):

$$\int_0^\infty \rho[f_{\mu,\nu} g_{\mu,\nu'} + f_{\mu,\nu'} g_{\mu,\nu}]d\rho = C\,\delta_{\nu,\nu'}, \tag{A3}$$

with C being the normalization constant.

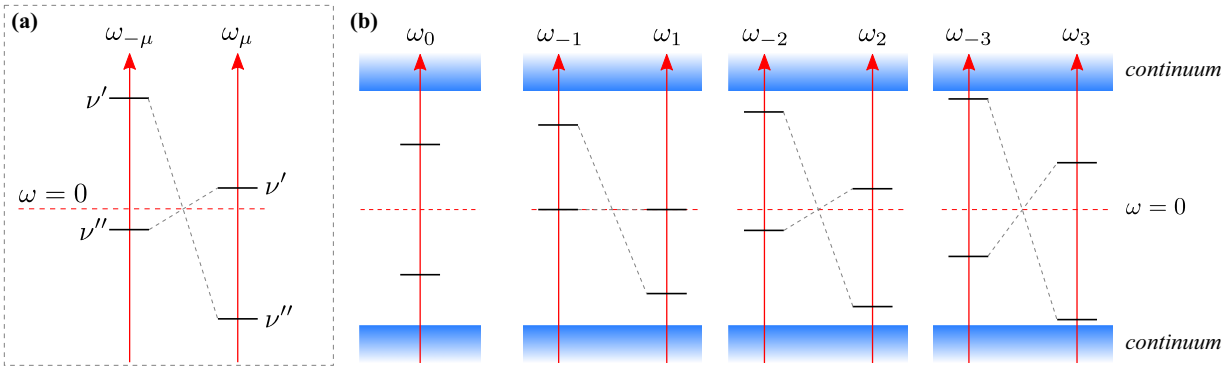

FIG. 4. Schematics of the magnon spectrum. (a) The symmetry between branches μ and $-\mu$ (only one pair $\{\nu',\nu''\}$ is shown). (b) The structure of the localized mode spectrum for $|\mu| \leqslant 3$.

Assuming that for all μ the EVP (A1) has no degenerate eigenvalues, one can present the general solution of (10) in the form of a partial wave expansion:

$$\vartheta = \sum_{\mu=-\infty}^{\infty} \sum_{\nu} f_{\mu,\nu}(\rho)[\bar{A}_{\mu,\nu}\cos(\mu\chi + \omega_{\mu,\nu}\tau) - \bar{B}_{\mu,\nu}\sin(\mu\chi + \omega_{\mu,\nu}\tau)],$$
$$\varphi = \sum_{\mu=-\infty}^{\infty} \sum_{\nu} g_{\mu,\nu}(\rho)[\bar{A}_{\mu,\nu}\sin(\mu\chi + \omega_{\mu,\nu}\tau) + \bar{B}_{\mu,\nu}\cos(\mu\chi + \omega_{\mu,\nu}\tau)]. \quad \text{(A4)}$$

Equation (A1) is invariant with respect to the simultaneous transformation $\omega_\mu \to -\omega_{-\mu}$, $f_\mu \to f_{-\mu}$, $g_\mu \to -g_{-\mu}$, and $\mu \to -\mu$. This means that the ν spectra can be split into the pairs $\bar{\nu} = \{\nu',\nu''\}$, which have the properties $\omega_{\mu,\nu'} = -\omega_{-\mu,\nu''}$, $f_{\mu,\nu'} = f_{-\mu,\nu''}$, and $g_{\mu,\nu'} = -g_{-\mu,\nu''}$. This symmetry is schematically shown in Fig. 4(a).

It can be used to present the general solution in a form which coincides with (A4), but (i) summation over ν is replaced by summation over pairs $\bar{\nu} = \{\nu',\nu''\}$, and for each pair only one index $\nu \in \{\nu',\nu''\}$ is chosen, which corresponds to a *certain sign of the frequency* $\omega_{\mu,\nu}$, and (ii) $\bar{A}_{\mu,\nu} \to A_{\mu\nu} = \bar{A}_{\mu,\nu'} + \bar{A}_{-\mu,\nu''}$ and $\bar{B}_{\mu,\nu} \to B_{\mu\nu} = \bar{B}_{\mu,\nu'} - \bar{B}_{-\mu,\nu''}$.

Analyzing numerically the spectrum of the EVP (A1), we found a number of localized modes with $|\omega_{\mu,\nu}| < 1$. Remarkably, for each given μ there is no more than one pair $\bar{\nu} = \{\nu',\nu''\}$ which corresponds to the localized modes [see Fig. 4(b)]. This fact and the above-described possibility to fix the sign of the frequency permit us to omit index ν when classifying the localized modes. Thus, in the following we consider that for each given μ there is no more than one localized mode with eigenfunctions $f_\mu(\rho)$, $g_\mu(\rho)$ and eigenfrequency $\omega_\mu \geqslant 0$ (the equality holds only for $\mu = 1$). Several examples of eigenfunctions are shown in Fig. 3.

The eigenfunctions have a number of useful properties. First of all, for the case of the localized modes, the previously described symmetry between branches μ and $-\mu$ can be used to write the orthogonality condition (A3) in the form of (12). The next important property can be described by integral relations between the eigenfrequencies and the eigenfunctions:

$$\omega_\mu = \frac{\varepsilon_\mu^f}{\alpha_\mu} = \frac{\varepsilon_\mu^g}{\alpha_\mu} = \frac{\kappa_\mu^f}{\beta_\mu} = \frac{\kappa_\mu^g}{\beta_\mu}. \quad \text{(A5)}$$

Here, the condition

$$\varepsilon_\mu^f = \varepsilon_\mu^g, \quad \text{(A6)}$$

where

$$\varepsilon_\mu^f = \int_0^\infty \rho\left[f_\mu'^2 + \left(\frac{\mu^2}{\rho^2} + U_1\right)f_\mu^2 + \mu W f_\mu g_\mu\right]d\rho,$$
$$\varepsilon_\mu^g = \int_0^\infty \rho\left[g_\mu'^2 + \left(\frac{\mu^2}{\rho^2} + U_2\right)g_\mu^2 + \mu W f_\mu g_\mu\right]d\rho \quad \text{(A7)}$$

mean that the energy is equally distributed between the f and g components of the mode. The condition

$$\kappa_\mu^f = \kappa_\mu^g, \quad \text{(A8)}$$

where

$$\kappa_\mu^f = \int_0^\infty \rho\left[f_\mu' f_{-\mu}' + \left(\frac{\mu^2}{\rho^2} + U_1\right)f_\mu f_{-\mu} + \mu W f_{-\mu} g_\mu\right]d\rho,$$
$$\kappa_\mu^g = \int_0^\infty \rho\left[g_\mu' g_{-\mu}' + \left(\frac{\mu^2}{\rho^2} + U_2\right)g_\mu g_{-\mu} + \mu W f_\mu g_{-\mu}\right]d\rho, \quad \text{(A9)}$$

results in the absence of coupling between modes $|\mu\rangle$ and $|-\mu\rangle$. Here,

$$\alpha_\mu = \int_0^\infty \rho f_\mu g_\mu d\rho, \quad \beta_\mu = \int_0^\infty \rho f_\mu g_{-\mu} d\rho. \quad \text{(A10)}$$

Note that $\beta_\mu = \beta_{-\mu}$, while $\alpha_\mu \neq \alpha_{-\mu}$. For the translational mode one has $\alpha_1 = 2$ and also

$$\varepsilon_1^f = \varepsilon_1^g = \kappa_1^f = \kappa_1^g = 0, \quad \text{(A11)}$$

which results in zero eigenfrequency $\omega_1 = 0$.

Properties (A5), (A6), (A8), and (A11) directly follow from Eqs. (11), which have the explicit form

$$-\nabla_\rho^2 f_\mu + \left(\frac{\mu^2}{\rho^2} + U_1\right)f_\mu + \mu W g_\mu = \omega_\mu g_\mu, \quad \text{(A12a)}$$
$$-\nabla_\rho^2 g_\mu + \left(\frac{\mu^2}{\rho^2} + U_2\right)g_\mu + \mu W f_\mu = \omega_\mu f_\mu. \quad \text{(A12b)}$$

Using integration by parts, one can present the quantity ε_μ^f in the form

$$\varepsilon_\mu^f = \int_0^\infty \rho\left[-\nabla_\rho^2 f_\mu + \left(\frac{\mu^2}{\rho^2} + U_1\right) f_\mu + \mu W g_\mu\right] f_\mu d\rho. \tag{A13}$$

Applying (A12a), one obtains $\varepsilon_\mu^f = \omega_\mu \alpha_\mu$. In a similar way, using (A12b), one obtains $\varepsilon_\mu^g = \omega_\mu \alpha_\mu$. Property (A8) can be proved analogously by applying the same procedure for the quantities κ_μ^f and κ_μ^g. Property (A11) can be checked straightforwardly by substituting into (A12) the explicit form of the eigenfunctions $f_1 = -\Theta'$ and $g_1 = \sin\Theta/\rho$. Properties (12), (A6), (A8), (A5), and (A11) have been verified numerically.

In order to estimate the asymptotic behavior of the eigenfrequencies for the case $R_s \gg 1$ we apply the variational approach [38] with the following trial functions:

$$f_\mu = \frac{a_\mu}{\cosh\frac{\rho-R_s}{|\delta|}}, \quad g_\mu = \frac{b_\mu}{\rho\cosh\frac{\rho-R_s}{|\delta|}}. \tag{A14}$$

Substituting (A14) into (A6), one obtains

$$\begin{aligned}\varepsilon_\mu^f &\approx \frac{2}{R_s}\left(\mu^2 a_\mu^2 - \mu a_\mu b_\mu\right) + \mathcal{C}_\mu^f \frac{a_\mu^2}{R_s^3} + \mu\mathcal{C}\frac{a_\mu b_\mu}{R_s^3},\\ \varepsilon_\mu^g &\approx \frac{2}{R_s}\left(b_\mu^2 - \mu a_\mu b_\mu\right) + \mathcal{C}_\mu^g \frac{b_\mu^2}{R_s^3} + \mu\mathcal{C}\frac{a_\mu b_\mu}{R_s^3}.\end{aligned} \tag{A15}$$

Generally, $\mathcal{C}_\mu^f \neq \mathcal{C}_\mu^g$. This means that for the ansatz (A14) the conditions $\varepsilon_\mu^f = \varepsilon_\mu^g$ and $\varepsilon_1^f = \varepsilon_1^g = 0$ can be satisfied simultaneously only with accuracy $\mathcal{O}(R_s^{-3})$. In this case $b_\mu = |\mu| a_\mu$. Using now the expressions for eigenfrequencies (A5) and taking into account that $\alpha_\mu \approx 2\delta a_\mu b_\mu$, one obtains $\omega_\mu \approx 2|\mu| R_s^{-1}$ when $\mu < 0$ and $\omega_\mu \approx c_\mu R_s^{-3}$ when $\mu > 0$. The constant c_μ cannot be determined from the model (A14). Comparison with the numerical solution leads to the estimate $c_\mu = \mu(\mu^2 - 1)/2$.

APPENDIX B: GENERALIZED SCHRÖDINGER EQUATION

Introducing the function $\psi = \vartheta + i\varphi$, one can write (10) in the form of the so-called generalized Schrödinger equation [39,58],

$$-i\partial_\tau \psi = \mathscr{H}\psi + \mathcal{W}\psi^\star, \quad \mathscr{H} = (-i\nabla - \boldsymbol{A})^2 + \mathcal{U}, \tag{B1}$$

with the potentials

$$\begin{aligned}\boldsymbol{A}(\rho) &= A\boldsymbol{e}_\chi, \quad A = -\frac{\cos\Theta}{\rho} + \frac{|d|}{2}\sin\Theta,\\ \mathcal{U}(\rho) &= \frac{U_1 + U_2}{2} - A^2,\\ \mathcal{W}(\rho) &= \frac{U_1 - U_2}{2}.\end{aligned} \tag{B2}$$

The vector function $\boldsymbol{A}$ acts as a vector potential of the effective magnetic field with the flux density

$$\boldsymbol{B} = \nabla\times\boldsymbol{A} = B\hat{\boldsymbol{z}}, \quad B = \frac{\left(-\cos\Theta + \frac{|d|}{2}\rho\sin\Theta\right)'}{\rho}. \tag{B3}$$

The first term in (B3) is the gyrocoupling density; finally, the total flux is determined by the π_2 homotopy group for the topological properties of the skyrmion (cf. Ref. [58])

$$\Phi = \int B\, d^2x = -4\pi\mathcal{Q}. \tag{B4}$$

[1] J. P. Liu, Z. Zhang, and G. Zhao, *Skyrmions: Topological Structures, Properties, and Applications*, Series in Materials Science and Engineering (CRC Press, Boca Raton, FL, 2016).

[2] *Topological Structures in Ferroic Materials*, edited by J. Seidel (Springer International Publishing, Switzerland, 2016).

[3] R. Wiesendanger, Nanoscale magnetic skyrmions in metallic films and multilayers: A new twist for spintronics, Nat. Rev. Mater. **1**, 16044 (2016).

[4] N. Nagaosa and Y. Tokura, Topological properties and dynamics of magnetic skyrmions, Nat. Nanotechnol. **8**, 899 (2013).

[5] A. O. Leonov, T. L. Monchesky, N. Romming, A. Kubetzka, A. N. Bogdanov, and R. Wiesendanger, The properties of isolated chiral skyrmions in thin magnetic films, New J. Phys. **18**, 065003 (2016).

[6] A. N. Bogdanov and D. A. Yablonskiĭ, Thermodynamically stable "vortices" in magnetically ordered crystals. The mixed state of magnets, JETP **68**, 101 (1989).

[7] A. Bogdanov and A. Hubert, Thermodynamically stable magnetic vortex states in magnetic crystals, J. Magn. Magn. Mater. **138**, 255 (1994).

[8] A. N. Bogdanov and U. K. Rößler, Chiral Symmetry Breaking in Magnetic Thin Films and Multilayers, Phys. Rev. Lett. **87**, 037203 (2001).

[9] B. A. Ivanov, V. A. Stephanovich, and A. A. Zhmudskii, Magnetic vortices—The microscopic analogs of magnetic bubbles, J. Magn. Magn. Mater. **88**, 116 (1990).

[10] *Electromagnetic, Magnetostatic, and Exchange-Interaction Vortices in Confined Magnetic Structures*, edited by E. Kamenetskii (Research Signpost, Kerala, India, 2008).

[11] F. G. Mertens and A. R. Bishop, Dynamics of vortices in two-dimensional magnets, in *Nonlinear Science at the Dawn of the 21st Century*, edited by P. L. Christiansen, M. P. Soerensen, and A. C. Scott (Springer, Berlin, 2000), pp. 137–170.

[12] N. Papanicolaou and T. N. Tomaras, Dynamics of magnetic vortices, Nucl. Phys. B **360**, 425 (1991).

[13] A. Fert, V. Cros, and J. Sampaio, Skyrmions on the track, Nat. Nanotechnol. **8**, 152 (2013).

[14] J. Sampaio, V. Cros, S. Rohart, A. Thiaville, and A. Fert, Nucleation, stability and current-induced motion of isolated magnetic skyrmions in nanostructures, Nat. Nanotechnol. **8**, 839 (2013).

[15] X. Zhang, G. P. Zhao, H. Fangohr, J. P. Liu, W. X. Xia, J. Xia, and F. J. Morvan, Skyrmion-skyrmion and skyrmion-edge repulsions in skyrmion-based racetrack memory, Sci. Rep. **5**, 7643 (2015).

[16] S. Krause and R. Wiesendanger, Spintronics: Skyrmionics gets hot, Nat. Mater. **15**, 493 (2016).

[17] W. Kang, Y. Huang, C. Zheng, W. Lv, N. Lei, Y. Zhang, X. Zhang, Y. Zhou, and W. Zhao, Voltage controlled magnetic skyrmion motion for racetrack memory, Sci. Rep. **6**, 23164 (2016).

[18] A. V. Chumak, V. I. Vasyuchka, A. A. Serga, and B. Hillebrands, Magnon spintronics, Nat. Phys. **11**, 453 (2015).

[19] A. V. Chumak, A. A. Serga, and B. Hillebrands, Magnon transistor for all-magnon data processing, Nat. Commun. **5**, 4700 (2014).

[20] T. Schneider, A. A. Serga, B. Leven, B. Hillebrands, R. L. Stamps, and M. P. Kostylev, Realization of spin-wave logic gates, Appl. Phys. Lett. **92**, 022505 (2008).

[21] O. Klein, G. de Loubens, V. V. Naletov, F. Boust, T. Guillet, H. Hurdequint, A. Leksikov, A. N. Slavin, V. S. Tiberkevich, and N. Vukadinovic, Ferromagnetic resonance force spectroscopy of individual submicron-size samples, Phys. Rev. B **78**, 144410 (2008).

[22] V. Castel, J. Ben Youssef, F. Boust, R. Weil, B. Pigeau, G. de Loubens, V. V. Naletov, O. Klein, and N. Vukadinovic, Perpendicular ferromagnetic resonance in soft cylindrical elements: Vortex and saturated states, Phys. Rev. B **85**, 184419 (2012).

[23] V. Novosad, F. Y. Fradin, P. E. Roy, K. S. Buchanan, K. Y. Guslienko, and S. D. Bader, Magnetic vortex resonance in patterned ferromagnetic dots, Phys. Rev. B **72**, 024455 (2005).

[24] C. Schütte and M. Garst, Magnon-skyrmion scattering in chiral magnets, Phys. Rev. B **90**, 094423 (2014).

[25] S.-Z. Lin, C. D. Batista, and A. Saxena, Internal modes of a skyrmion in the ferromagnetic state of chiral magnets, Phys. Rev. B **89**, 024415 (2014).

[26] J. Iwasaki, A. J. Beekman, and N. Nagaosa, Theory of magnon-skyrmion scattering in chiral magnets, Phys. Rev. B **89**, 064412 (2014).

[27] S. Schroeter and M. Garst, Scattering of high-energy magnons off a magnetic skyrmion, Low Temp. Phys. **41**, 1043 (2015).

[28] M. Garst, J. Waizner, and D. Grundler, Collective spin excitations of helices and magnetic skyrmions: Review and perspectives of magnonics in non-centrosymmetric magnets, J. Phys. D **50**, 293002 (2017).

[29] I. Makhfudz, B. Krüger, and O. Tchernyshyov, Inertia and Chiral Edge Modes of a Skyrmion Magnetic Bubble, Phys. Rev. Lett. **109**, 217201 (2012).

[30] F. J. Buijnsters, A. Fasolino, and M. I. Katsnelson, Zero modes in magnetic systems: General theory and an efficient computational scheme, Phys. Rev. B **89**, 174433 (2014).

[31] V. L. Zhang, C. G. Hou, K. Di, H. S. Lim, S. C. Ng, S. D. Pollard, H. Yang, and M. H. Kuok, Eigenmodes of Néel skyrmions in ultrathin magnetic films, AIP Adv. **7**, 055212 (2017).

[32] M. Mruczkiewicz, M. Krawczyk, and K. Y. Guslienko, Spin excitation spectrum in a magnetic nanodot with continuous transitions between the vortex, Bloch-type skyrmion, and Néel-type skyrmion states, Phys. Rev. B **95**, 094414 (2017).

[33] K. Y. Guslienko and Z. V. Gareeva, Gyrotropic skyrmion modes in ultrathin magnetic circular dots, IEEE Magn. Lett. **8**, 1 (2017).

[34] A. R. Völkel, G. M. Wysin, F. G. Mertens, A. R. Bishop, and H. J. Schnitzer, Collective-variable approach to the dynamics of nonlinear magnetic excitations with application to vortices, Phys. Rev. B **50**, 12711 (1994).

[35] F. G. Mertens, H. J. Schnitzer, and A. R. Bishop, Hierarchy of equations of motion for nonlinear coherent excitations applied to magnetic vortices, Phys. Rev. B **56**, 2510 (1997).

[36] G. M. Wysin, Magnetic vortex mass in two-dimensional easy-plane magnets, Phys. Rev. B **54**, 15156 (1996).

[37] B. A. Ivanov, H. J. Schnitzer, F. G. Mertens, and G. M. Wysin, Magnon modes and magnon-vortex scattering in two-dimensional easy-plane ferromagnets, Phys. Rev. B **58**, 8464 (1998).

[38] D. D. Sheka, B. A. Ivanov, and F. G. Mertens, Internal modes and magnon scattering on topological solitons in two-dimensional easy-axis ferromagnets, Phys. Rev. B **64**, 024432 (2001).

[39] B. A. Ivanov and D. D. Sheka, Local magnon modes and the dynamics of a small-radius two-dimensional magnetic soliton in an easy-axis ferromagnet, JETP Lett. **82**, 436 (2005).

[40] D. D. Sheka, C. Schuster, B. A. Ivanov, and F. G. Mertens, Dynamics of topological solitons in two-dimensional ferromagnets, Eur. Phys. J. B **50**, 393 (2006).

[41] F. Büttner, C. Moutafis, M. Schneider, B. Krüger, C. M. Günther, J. Geilhufe, C. v. Korff Schmising, J. Mohanty, B. Pfau, S. Schaffert, A. Bisig, M. Foerster, T. Schulz, C. A. F. Vaz, J. H. Franken, H. J. M. Swagten, M. Kläui, and S. Eisebitt, Dynamics and inertia of skyrmionic spin structures, Nat. Phys. **11**, 225 (2015).

[42] S. Rohart and A. Thiaville, Skyrmion confinement in ultrathin film nanostructures in the presence of Dzyaloshinskii-Moriya interaction, Phys. Rev. B **88**, 184422 (2013).

[43] G. Gioia and R. D. James, Micromagnetics of very thin films, Proc. R. Soc. London, Ser. A **453**, 213 (1997).

[44] R. V. Kohn and V. V. Slastikov, Effective dynamics for ferromagnetic thin films: A rigorous justification, Proc. R. Soc. London, Ser. A **461**, 143 (2005).

[45] A. Crépieux and C. Lacroix, Dzyaloshinsky-Moriya interactions induced by symmetry breaking at a surface, J. Magn. Magn. Mater. **182**, 341 (1998).

[46] A. Thiaville, S. Rohart, É. Jué, V. Cros, and A. Fert, Dynamics of Dzyaloshinskii domain walls in ultrathin magnetic films, Europhys. Lett. **100**, 57002 (2012).

[47] H. Yang, A. Thiaville, S. Rohart, A. Fert, and M. Chshiev, Anatomy of Dzyaloshinskii-Moriya Interaction at Co/Pt interfaces, Phys. Rev. Lett. **115**, 267210 (2015).

[48] I. E. Dzialoshinskii, Thermodynamic theory of "weak" ferromagnetism in antiferromagnetic substances, Sov. Phys. JETP **5**, 1259 (1957).

[49] I. E. Dzyaloshinskii, Theory of helicoidal structures in antiferromagnets. I. Nonmetals, Sov. Phys. JETP **19**, 964 (1964).

[50] A. A. Belavin and A. M. Polyakov, Metastable states of a 2D isotropic ferromagnet, JETP Lett. **22**, 245 (1975).

[51] I. E. Dzyaloshinskii, The theory of helicoidal structures in antiferromagnets. II. Metals, Sov. Phys. JETP **20**, 223 (1965).

[52] S. Komineas and N. Papanicolaou, Skyrmion dynamics in chiral ferromagnets, Phys. Rev. B **92**, 064412 (2015).

[53] D. J. Clarke, O. A. Tretiakov, G.-W. Chern, Y. B. Bazaliy, and O. Tchernyshyov, Dynamics of a vortex domain wall in a magnetic nanostrip: Application of the collective-coordinate approach, Phys. Rev. B **78**, 134412 (2008).

[54] *Spin Dynamics in Confined Magnetic Structures III*, edited by B. Hillebrands and A. Thiaville, Topics in Applied Physics Vol. 101 (Springer, Berlin, 2006).

[55] N. L. Schryer and L. R. Walker, The motion of 180° domain walls in uniform dc magnetic fields, J. Appl. Phys. **45**, 5406 (1974).

[56] A. Thiaville, J. M. Garcia, and J. Miltat, Domain wall dynamics in nanowires, J. Magn. Magn. Mater. **242–245**, 1061 (2002).
[57] A. P. Malozemoff and J. C. Slonzewski, *Magnetic Domain Walls in Bubble Materials* (Academic Press, New York, 1979).
[58] D. D. Sheka, I. A. Yastremsky, B. A. Ivanov, G. M. Wysin, and F. G. Mertens, Amplitudes for magnon scattering by vortices in two-dimensional weakly easy-plane ferromagnets, Phys. Rev. B **69**, 054429 (2004).
[59] The property $\omega_1 = 0$ can be verified by direct substitution of the eigenfunctions into (11).
[60] A. Bogdanov and A. Hubert, The stability of vortex-like structures in uniaxial ferromagnets, J. Magn. Magn. Mater. **195**, 182 (1999).
[61] A. Bogdanov and A. Hubert, The properties of isolated magnetic vortices, Phys. Status Solidi B **186**, 527 (1994).
[62] R. Rajaraman, *Solitons and Instanton* (North-Holland, Amsterdam, 1982).
[63] A. A. Thiele, Steady-State Motion of Magnetic of Magnetic Domains, Phys. Rev. Lett. **30**, 230 (1973).
[64] A. A. Thiele, Applications of the gyrocoupling vector and dissipation dyadic in the dynamics of magnetic domains, J. Appl. Phys. **45**, 377 (1974).
[65] A. Hubert and R. Schäfer, *Magnetic Domains: The Analysis of Magnetic Microstructures* (Springer, Berlin, 1998).
[66] For the considered boundary conditions (3b) one has $\mathcal{Q} = 1$.
[67] N. Papanicolaou and W. J. Zakrzewski, Dynamics of interacting magnetic vortices in a model Landau-Lifshitz equation, Phys. D (Amsterdam, Neth.) **80**, 225 (1995).
[68] N. Papanicolaou and W. J. Zakrzewski, Dynamics of magnetic bubbles in a Skyrme model, Phys. Lett. A **210**, 328 (1996).
[69] S. Komineas and N. Papanicolaou, Topology and dynamics in ferromagnetic media, Phys. D (Amsterdam, Neth.) **99**, 81 (1996).
[70] N. Papanicolaou and P. N. Spathis, Semitopological solitons in planar ferromagnets, Nonlinearity **12**, 285 (1999).
[71] A. V. Nikiforov and É. B. Sonin, Dynamics of magnetic vortices in a planar ferromagnet, Sov. Phys. JETP **58**, 373 (1983).
[72] H. Velkov, O. Gomonay, M. Beens, G. Schwiete, A. Brataas, J. Sinova, and R. A. Duine, Phenomenology of current-induced skyrmion motion in antiferromagnets, New J. Phys. **18**, 075016 (2016).
[73] A. K. Zvezdin and K. A. Zvezdin, Magnus force and the inertial properties of magnetic vortices in weak ferromagnets, Low Temp. Phys. **36**, 826 (2010).
[74] I. V. Bar'yakhtar and B. A. Ivanov, Nonlinear magnetization waves in the antiferromagnet, Sov. J. Low Temp. Phys. **5**, 361 (1979).
[75] A. F. Andreev and V. I. Marchenko, Symmetry and macroscopical dynamics of a magnet, Sov. Phys. Usp. **23**, 21 (1980).
[76] K. M. D. Hals, Y. Tserkovnyak, and A. Brataas, Phenomenology of Current-Induced Dynamics in Antiferromagnets, Phys. Rev. Lett. **106**, 107206 (2011).
[77] E. V. Gomonay and V. M. Loktev, Spintronics of antiferromagnetic systems (review article), Low Temp. Phys. **40**, 17 (2014).
[78] B. A. Ivanov and V. A. Stephanovich, Two-dimensional soliton dynamics in ferromagnets, Phys. Lett. A **141**, 89 (1989).
[79] S.-Z. Lin, Dynamics and inertia of a skyrmion in chiral magnets and interfaces: A linear response approach based on magnon excitations, Phys. Rev. B **96**, 014407 (2017).
[80] C. Psaroudaki, S. Hoffman, J. Klinovaja, and D. Loss, Quantum Dynamics of Skyrmions in Chiral Magnets, Phys. Rev. X **7**, 041045 (2017).